

Hazard Assessment Comparison of Tazhiping Landslide Before and After Treatment using finite volume method

Dong Huang^{1*}, YuanJun Jiang^{1*}, JianPing Qiao¹, Meng Wang¹

1. Key Laboratory of Mountain hazards and Surface process, Institute of Mountain hazards and Environment, Chinese Academy of Science, Chengdu 610041, China

*Corresponding author (yuanjun.jiang.civil@gmail.com).

Abstract: Through investigation and analysis of geological conditions and mechanical parameters of the Taziping landslide, the finite volume method was adopted, and, the rheological model was adopted to simulate the landslide and avalanche entire mass movement process. The present paper adopted the numerical approach in RAMMS and the GIS platform to simulate the mass movement process before and after treatment. This paper also provided the conditions and characteristic parameters of soil deposits (flow height, velocity, and stresses) during the landslide mass movement process and mapped the 3D division of hazard zones before and after landslide treatment. Results indicated that the scope of hazard zones contracted after engineering treatment of the landslide. The extent of high-hazard zones was reduced by about 2/3 of the area before treatment, and characteristic parameters of the mass movement process after treatment decreased to 1/3 of those before treatment. Despite engineering treatment, the Taziping landslide still poses significant hazard to nearby settlements. Therefore, we propose that houses located in high-hazard zones be relocated or reinforced for protection.

Keywords: finite volume method; rheological model; motion feature parameters; hazard assessment

1. Introduction

The hazards of a landslide include scope of influence (i.e., source area, possible path area, and backward and lateral expansion area) and secondary disasters (i.e., reservoir surge, blast, and landslide-induced barrier lake). A typical landslide hazard assessment aims to propose a systematic hazard assessment method with regard to a given position or a potential landslide. Current research on typical landslide hazard assessment remains immature, and there are multiple methods for interpreting landslide hazards. To be specific, the scope of influence prediction of a landslide refers to deformation and instability characteristics such as sliding distance, movement speed, and bulking thickness range. The movement behavior of a landslide mass is related to its occurrence, sliding mechanisms, mass characteristics, sliding path, and many other factors. Current landslide movement prediction methods include empirical prediction and numerical simulation.

Empirical prediction method: The empirical prediction method involves

44 analyzing landslide flow through the collection of landslide parameters in the field. It
45 further consists of the geomorphologic method (Costa, 1984; Jackson et al., 1987;
46 Scott et al., 1993), the geometric change method (Finlay et al., 1999; Michael-Leiba et
47 al., 2003), and the volume change method (Fannin et al., 2001). Empirical models are
48 commonly simple and easy to apply, and the required data are easy to obtain as well.
49 **Numerical simulation method:** Numerical simulation methods are further divided
50 into the continuous deformation analysis method (Hung, 1995; Evans et al., 2009;;
51 Wang, et al., 2016), the discontinuous deformation analysis method (Shi, 1988;), and
52 the simplified analytical simulation method (Christen et al., 2010a; Sassa, 2010;
53 Bartelt et al., 2012; Du et al., 2015). The numerical simulation method expresses
54 continuous physical variables using the original spatial and temporal coordinates with
55 geometric values of discrete points. Numerical simulations follow certain rules to
56 establish an algebraic equation set in order to obtain approximate solutions for
57 physical variables.

58 Empirical prediction models only provide a simple prediction of the sliding path.
59 Due to the differences in geological environments, empirical prediction models
60 commonly have low generality. The continuous deformation method has the
61 advantage of an extremely strong replication capability, but it is not recommended
62 when analyzing flow-type landslides, lahars, or debris flows because of complicated
63 rheological behaviors (Iverson et al., 1997, 2001; Hung et al., 2001; Portilla et al.,
64 2010; Chen et al., 2014). The fluid mechanics-based discontinuous deformation
65 method has several shortcomings such as, great computational burden, difficult
66 parameter selection, and difficult 3D implementation. The simplified analytical
67 simulation method fully takes into account the flow state properties of landslides
68 before introducing a rheological model and can easily realize 3D implementation on
69 the GIS platform. On that account, this paper adopted the continuous fluid
70 mechanics-based finite volume method (simplified analytical simulation method). We
71 introduce a rheological model on the basis of using mass as well as momentum and
72 energy conservation to describe the movement of landslides. We also employed GIS
73 analysis to simulate the entire movement process of Taziping landslide and map the
74 2D division of hazard zones.

75

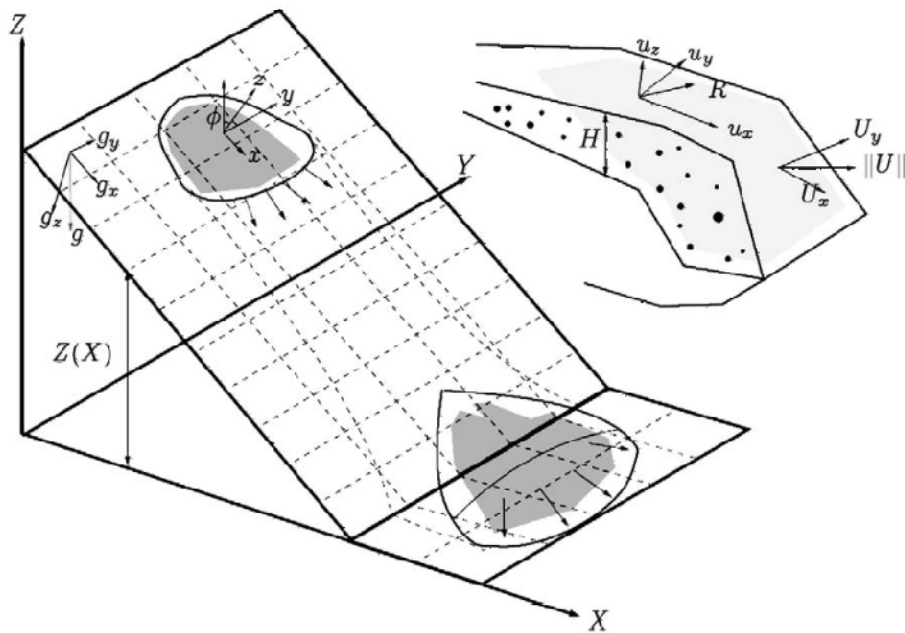
76 **2. Methods**

77 **2.1 Kinetic analysis method**

78 Adopting the continuous fluid mechanics-based finite volume method, this paper
79 took into account erosion action on the lower surface of the sliding mass and the
80 change in frictional resistance within the landslide-debris flow in order to establish a
81 computational model. The basic idea is to divide the calculation area into a series of
82 non-repetitive control volumes, ensuring that there is a control volume around each
83 grid point. Each control volume is then integrated by the unresolved differential
84 equation in order to obtain a set of discrete equations. The unknown variable is the
85 numerical value of the dependent variable at each grid point. To solve the integral of a
86 control volume, we make a hypothesis about the change rule of values among grid

87 points, that is, about their piecewise distribution profile. The finite volume method
 88 can satisfactorily overcome the finite element method's weakness of slow calculation,
 89 and solve the problem of complex region processing. Thus, we adopted the finite
 90 volume method to establish the kinematic model for the landslide flow process.

91 The core of the finite volume method is domain discretization. The finite volume
 92 method uses discrete points as a substitute for continuous space. The physical
 93 meaning of the discrete equation is the conservation of the dependent variable in a
 94 finite control volume. Establishment of the conservation equation is based on the
 95 continuous movement model, that is, the continuity hypothesis about landslide
 96 substances. We divided the landslide mass into a series of units and made the
 97 hypothesis that each unit has consistent kinematic parameters (speed at a depth,
 98 density, etc.) and physical parameters (Fig.1). We also established an Eulerian
 99 coordinate system-based conservation equation with regard to each control volume.



100

101 Fig.1 Schematic diagram of finite volume discretization (Christen et al., 2010a).

102 **2.2 Control equation**

103 The computational domain is defined as directions x and y , and the
 104 topographic elevation is given the coordinate $z(x, y)$. $H(x, y, t)$ is assumed as the
 105 change relationship of landslide thickness with time; $U_x(x, y, t)$ and $U_y(x, y, t)$
 106 respectively represent the mean movement speeds along directions x and y at
 107 moment t ; $n_x = U_x / \sqrt{U_x^2 + U_y^2}$ and $n_y = U_y / \sqrt{U_x^2 + U_y^2}$ represent the cosinoidal and
 108 sinusoidal flow vectors of the landslide on the plane $x - y$. The mean flow speed of

109 substances is defined as $U = \sqrt{U_x^2 + U_y^2}$.

110 Thus, the mass balance equation becomes:

$$111 \quad \partial_t H + \partial_x (HU_x) + \partial_y (HU_y) = \dot{Q} \quad (1)$$

112 wherein, $\dot{Q}(x, y, t)$ represents the change rate (entrainment rate) of landslide
113 volume with time.

114 Assuming that $l(x, y, t)$ represents the movement distance of the landslide with
115 time, we can obtain:

$$116 \quad \dot{Q} = \begin{cases} 0 & \text{if } h_i = 0 \\ \frac{\rho_i}{\rho_a} h_i \frac{U}{l} & \text{if } k_i l \geq h_i \\ \frac{\rho_i}{\rho_a} k_i U & \text{if } k_i l < h_i \end{cases} \quad (2)$$

117 wherein, h_i represents the thickness of the i th layer of the landslide in the
118 movement process; ρ_i represents the density of the i th layer of the landslide in the
119 movement process; ρ_a represents the density of the landslide; the dimensionless
120 parameter k_i represents the entrainment rate.

121 The momentum balance equation is:

$$122 \quad \partial_t (HU_x) + \partial_x (HU_x^2 + \frac{g_z k_{a/p} H^2}{2}) + \partial_y (HU_x U_y) = S_{gy} - S_f(R)[n_x] \quad (3)$$

$$123 \quad \partial_t (HU_y) + \partial_y (HU_y^2 + \frac{g_z k_{a/p} H^2}{2}) + \partial_x (HU_x U_y) = S_{gx} - S_f(R)[n_y] \quad (4)$$

124 wherein, $S_{gx} = g_x H$ and $S_{gy} = g_y H$ represent the dynamic components of the
125 acceleration of gravity in directions x and y ; $g = (g_x \ g_y \ g_z)$ represents the
126 vector of the acceleration of gravity; $k_{a/p}$ represents the pressure coefficient of soil;
127 ρ_a represents the density of the landslide; the dimensionless parameter k_i
128 represents the entrainment rate; $S_f(R)$ represents the frictional resistance.

129 The kinetic energy balance equation is:

$$130 \quad \partial_t (HR) + \partial_x (HRU_x) + \partial_y (HRU_y) = \dot{P} - \dot{D} \quad (5)$$

131 wherein, $R(x, y, t)$ represents the random mean kinetic energy of the landslide;
 132 $\dot{P}(x, y, t)$ and $\dot{D}(x, y, t)$ represent the random increased kinetic energy and decreased
 133 kinetic energy of the landslide.

134 2.3 Constitutive relationship

135 The improved Voellmy rheological model is applied in the computational
 136 simulation of the landslide. See the computational formula below:

$$137 \quad S_f = \frac{u_i}{\|U\|} (h\mu g_z + R_i U^2 + R_\zeta U^2) \quad (6)$$

$$138 \quad R_i = \mu h \frac{U^T K U}{U^2}, R_\zeta = \frac{g}{\zeta} \quad (7)$$

139 wherein, $u_i/\|U\|$ represents the unit vector in the movement direction of the
 140 landslide; μ represents the Coulomb friction coefficient, and is related to $R(x, y, t)$,
 141 the random mean kinetic energy of the landslide; R_i represents the gravity-related
 142 frictional force coefficient; K represents the substrate surface curvature; ζ
 143 represents the viscous friction coefficient of the ‘‘turbulent flow’’.

144 2.4 HLLE-Heun numerical solution

145 Synthesizing control equations (1), (3), (4) and (5), we can obtain the simplified
 146 form of the nonlinear hyperbola equation:

$$147 \quad \partial_t V + \nabla \cdot F(V) = G(V) \quad (8)$$

$$148 \quad V = \begin{pmatrix} H \\ HU_x \\ HU_y \\ HR \end{pmatrix} \quad G(V) := \begin{pmatrix} \dot{Q} \\ S_{gx} - S_{fx} \\ S_{gy} - S_{fy} \\ \dot{P} - \dot{D} \end{pmatrix}$$

$$149 \quad F(V) = \begin{pmatrix} HU_x & HU_y \\ HU_x^2 + g_z k_{al/p} \frac{H^2}{2} & HU_x U_y \\ HU_x U_y & HU_y^2 + g_z k_{al/p} \frac{H^2}{2} \\ HRU_x & HRU_y \end{pmatrix}$$

150 wherein, $V(x, y, t)$ represents a vector equation consisting of four unknown
 151 vector variables; $F(V)$ represents the flux function; $G(V)$ represents the source
 152 term. Based on the HLLE equation of the finite volume method and the quadrilateral
 153 grid, the node layout can adopt the grid center pattern, and the normal flux along one
 154 side of the control volume can be represented by the flux at the center of the side. The

155 finite volume discretization adopting the control volume as unit is depicted in Fig.1;
 156 the Gauss theorem can be followed for the integration of equation (8), wherein C_i
 157 represents the unit volume; after converting the volume integral flux function $F(V)$
 158 into the curved surface integral, we can obtain:

$$159 \quad \int_{C_i} \partial_t V dx + \oint_{\partial C_i} F(V) \cdot n_i d\sigma = \int_{C_i} G(V) dx \quad (9)$$

160 wherein, n_i represents the outward normal direction vertical to unit C_i at the
 161 boundary; through adopting the HLL format for the discretization of surface integral,
 162 the following simplified form can be obtained:

$$163 \quad V_i^{(*)} = V_i^{(n)} + \frac{\Delta t}{A_{C_i}} \Delta F_i^{(HLL)}(V^{(n)}) \quad (10)$$

$$164 \quad V_i^{(**)} = V_i^{(*)} + \frac{\Delta t}{A_{C_i}} \Delta F_i^{(HLL)}(V^{(*)}) \quad (11)$$

$$165 \quad V_i^{(n+1)} = \frac{1}{2} (V_i^{(n)} + V_i^{(**)}) \quad (12)$$

166 wherein, $V_i^{(n)}$ represents the mean value of unit variables at moment $t^{(n)}$; $V^{(n)}$
 167 represents the mean value of the entire grid at moment $t^{(n)}$; $\Delta t := t^{(n-1)} - t^{(n)}$ represents
 168 the calculated time step; A_{C_i} represents the area of unit C_i ; $\Delta F_i^{(HLL)}$ represents the
 169 approximate value of the curved surface integral, as shown below:

$$170 \quad \Delta F_i^{(HLL)}(V^{(n)}) := - \sum_{j=1}^4 F_{ij}^{(HLL)}(V^{(n)}) n_{ij} \Delta X \quad (13)$$

171 wherein, n_{ij} represents the outward normal direction of the i th unit at
 172 boundary j ; the flux calculation term $F_{ij}^{(HLL)}(V^{(n)})$ represents the approximate
 173 solution mode of the Riemann problem of the i th unit at boundary j ; see the
 174 computational formula below:

$$175 \quad F_{ij}^{(HLL)}(V^{(n)}) = \begin{cases} F(V_L^{(n)}) & 0 \leq S_L \\ \frac{S_R F(V_L^{(n)}) - S_L F(V_R^{(n)}) + S_R S_L F(V_R^{(n)} - V_L^{(n)})}{S_R - S_L} & S_L \leq 0 \leq S_R \\ F(V_R^{(n)}) & S_R \leq 0 \end{cases} \quad (14)$$

176 wherein, $V_L^{(n)}$ and $V_R^{(n)}$ respectively represent the approximate values of $V^{(n)}$

177 on both sides of boundary j of the i th unit; S_L and S_R respectively represent the
178 wave speeds on the left and right sides. Refer to the computational method described
179 by Toro (1992). In addition, the gradient magnitude in the original second-order
180 difference equation can be limited through multiplication with the flux limiter, and the
181 second-order format of the TVD property can be constructed to avoid the occurrence
182 of numerical oscillation. Refer to the specific method described by LeVeque (2002).

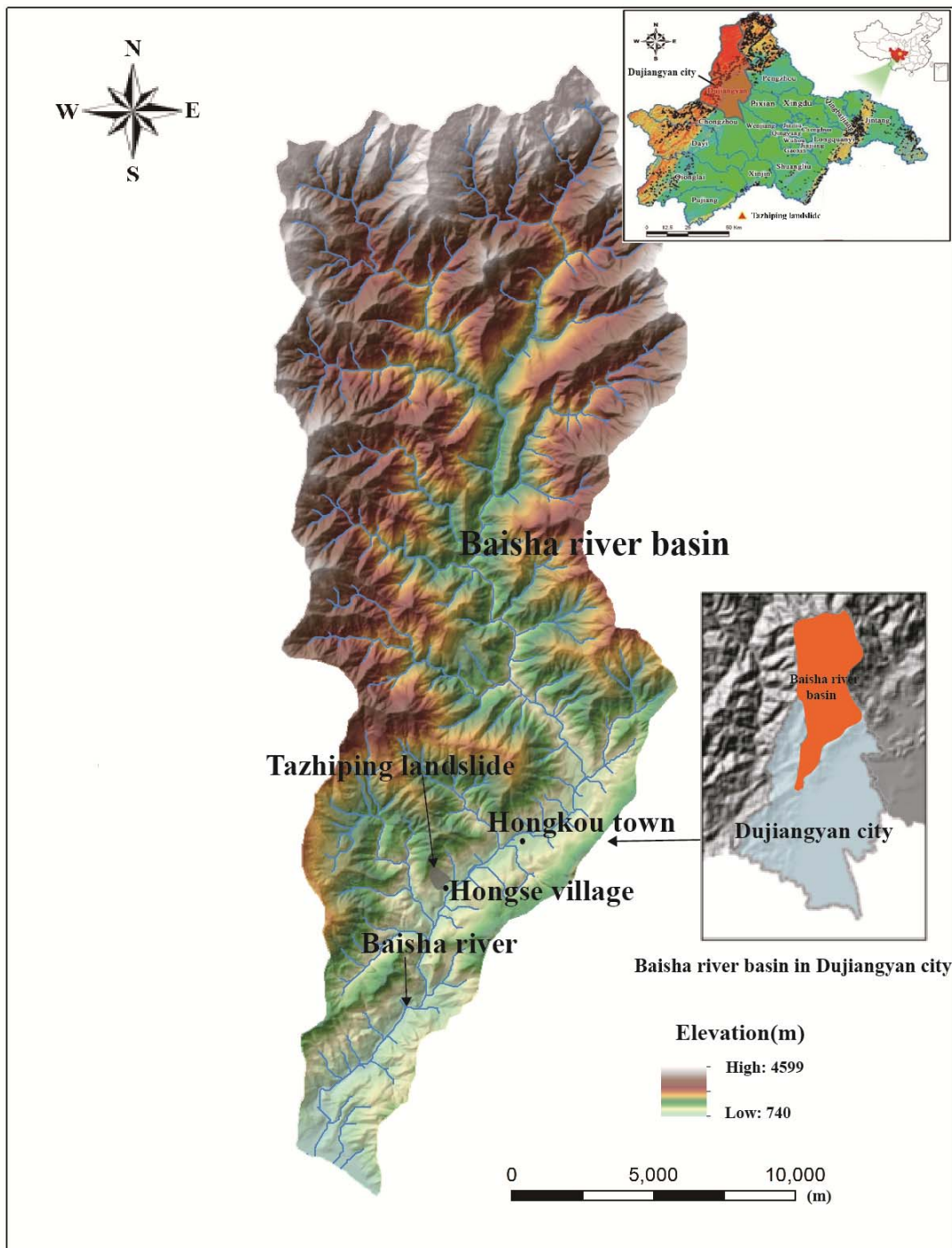
183 In this paper numerical solver used within RAMMS, which was specifically
184 designed to provide landslide(avalanche) engineers with a tool that can be applied to
185 analyze problems that two-dimensional depth-averaged mass and momentum
186 equations on three-dimensional terrain using both first and second-order finite volume
187 methods (Christen et al., 2010b).

188 **3. Study area and data**

189 **3.1 Taziping landslide**

190 Taziping landslide is located in the southeast of the Hongse Village, Hongkou
191 Town, Dujiangyan City of Sichuan Province. The site is located at (E103°37'46",
192 N31°6'29"), 68 km away from Chengdu City to the east and 20 km away from the
193 Dujiangyan Urban District (Fig. 2). Its geomorphic unit is a middle-mountain tectonic
194 erosion area, falling within the slope geomorphology on the right bank of the Baisha
195 River Valley. As an colluvial layer landslide triggered by the Wenchuan Earthquake,
196 Taziping Landslide is a large-scale landslide as shown in Fig. 3. It has a gradient of
197 25°-40° with an average of about 32°. The landslide has an apparent round-backed
198 armchair contour, and has formed a steep rear edge, which has a gradient of 35°-50°
199 and an elevation of about 1,370 m. The front edge is located on the south side of the
200 mountain road, and has an elevation of about 1,007 m. The landslide has an elevation
201 difference of about 363 m, and the main sliding direction of 124°NE. The landslide
202 mass is in an irregular semi-elliptical shape, and has a length of about 530 m, an
203 average width of 145 m and a landslide area of approximately $7.68 \times 10^4 \text{ m}^2$. The
204 landslide mass is gravelly soil in lithology, and is covered on the surface by silty clay
205 mingled with gravels. In terms of spatial distribution, it is thick in the middle and thin
206 on the lateral edges, and has a thickness of 20-25 m and a volume of approximately
207 $1.16 \times 10^6 \text{ m}^3$. During the earthquake, the landslide mass slid to cover the northern
208 mountain slope mass of the Hongse Village Miaoba settlement. The landslide has an
209 apparent front edge boundary, and there is also a swelling deformation (Fig. 4).

210

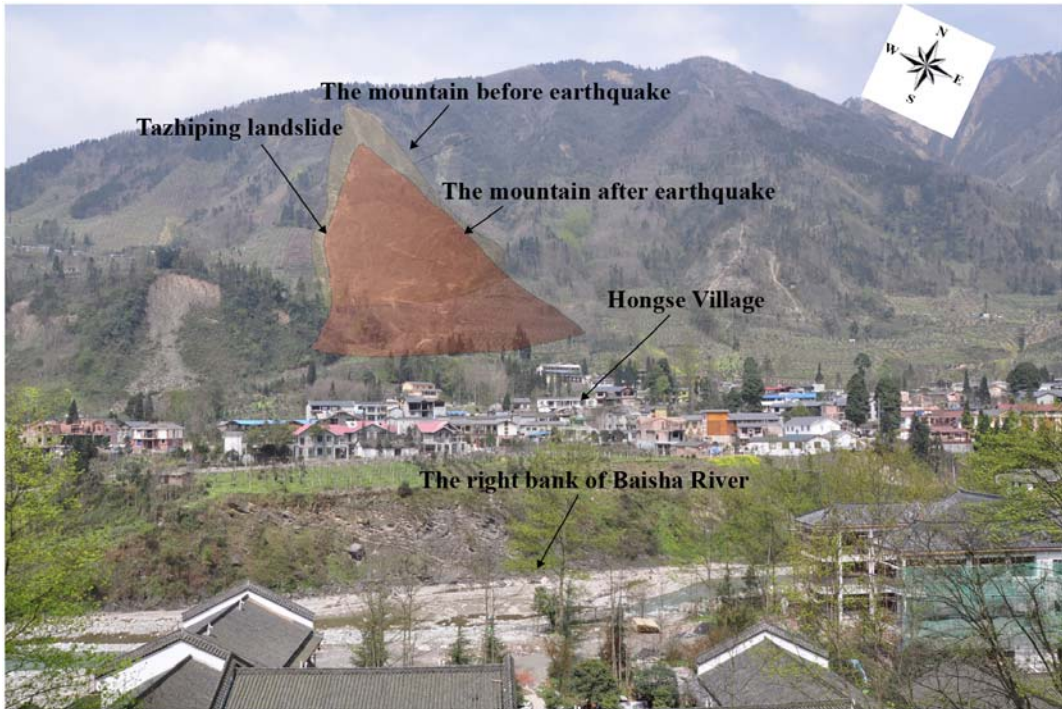


211

212

213

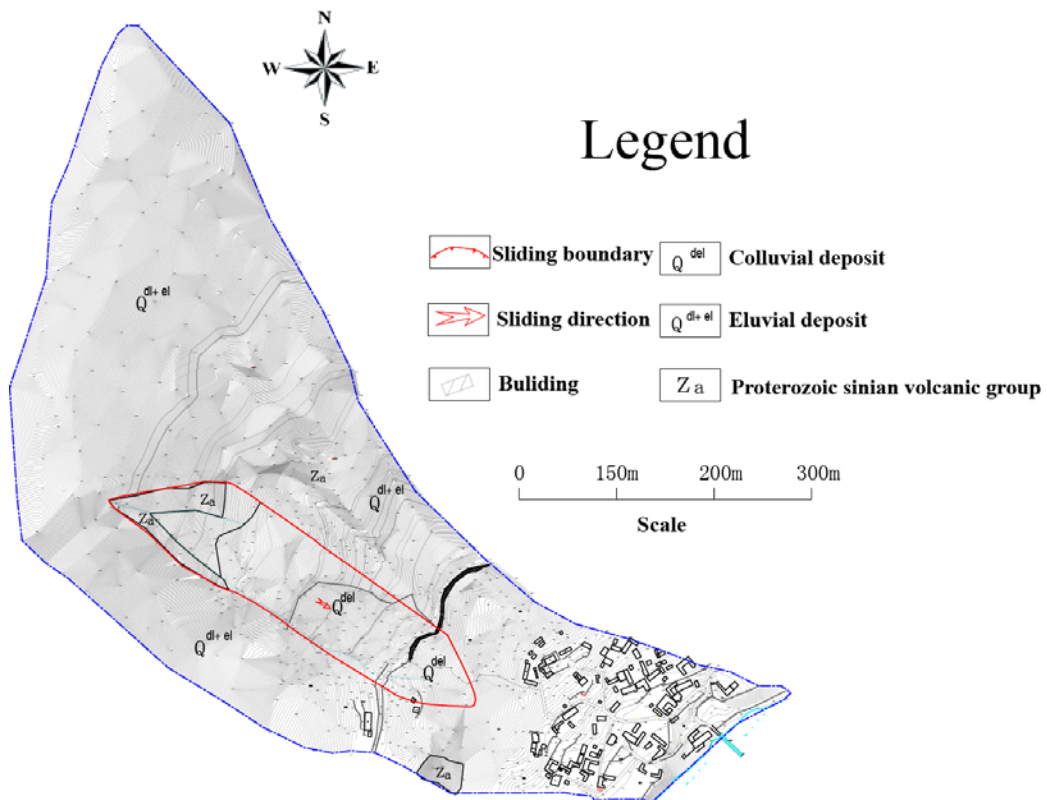
Fig.2 Location of Tazhiping landslide, Baisha river basin, Dujiangyan city (the landslide triggered by Wenchuan Ms 8.0 earthquake on May 12, 2008)



214

215

Fig.3 Tazhiping Landslide



216

217

Fig.4 Plane sketch of Tazhiping landslide

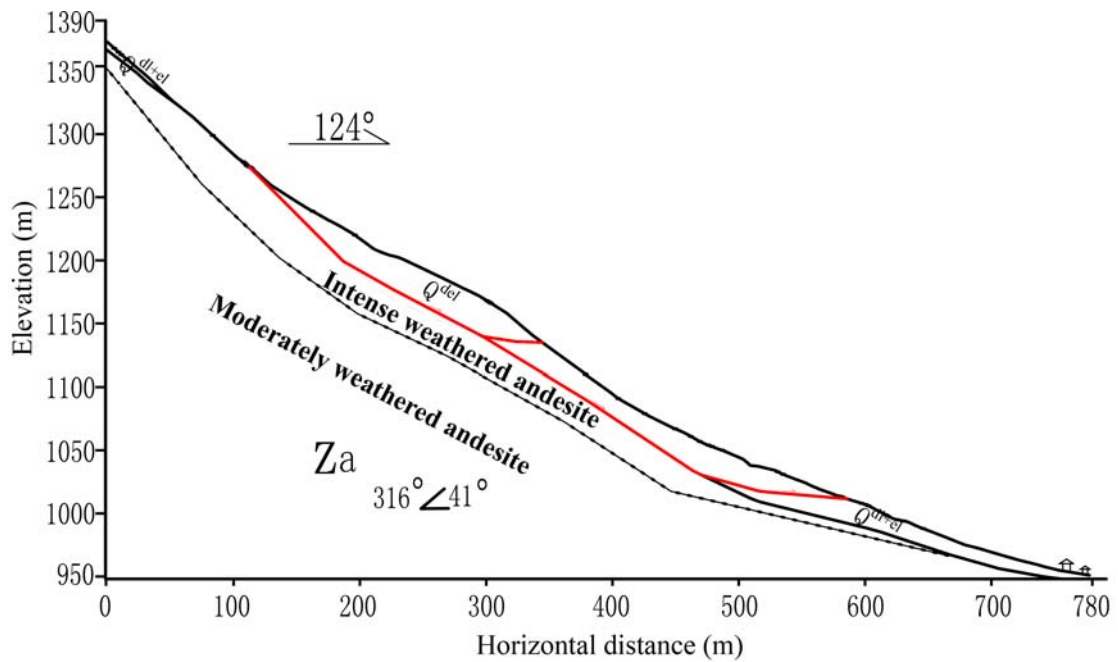
218

After Wenchuan Earthquake, the massive colluvial deposits covers on the
 219 mountain slope, and the landslide mass is dominated by the colluvium. The colluvium
 220 is mainly distributed on the top surface of the landslide mass in the thickness of

221 0.5-5.0 m, and is mainly constituted by rubbles and gravels. The mass consists of a
 222 small amount of fine gravel substances which are gray or grayish-green, and
 223 dominated by andesite in composition, generally with a block size of 20-150 cm.
 224 Field survey indicates that the rubbles in the surface layer have a maximum diameter
 225 exceeding 2 m, and that fine gravel substances are filled among rubbles in a loose
 226 structure. Within the thickness of 5-10 m, the landslide mass is constituted of a small
 227 amount of yellowish-brown and gray-brown silty clay mingled with 5-40% of
 228 non-uniformly distributed broken rubbles. Within the thickness of 10-25 m, there is a
 229 wide distribution of gravelly soil. The soil is grayish-green or variegated in color, is
 230 slightly compact and non-uniform, and has a broken stone content of about 50%. The
 231 parent rock of the broken stones is andesite, filled with silty clay or silt (Fig.5). Table
 232 1 shows the parameters of the surface gravelly soil of the landslide mass based on the
 233 field sampling.

234 Tab.1 Parameters of the surface soil of Taziping Landslide

Internal friction angle (°)		Cohesion (kPa)	Relative compactness	Natural void ratio	Dry density (kN·m ⁻³)	Specific gravity (g·cm ⁻³)
Peak	Residual					
27.5	23	20.5	53%	0.789	15.357	2.492



235 236

Fig.5 Geological profile of Taziping Landslide

237 The landslide is an unconsolidated mass containing relatively large amounts of
 238 crushed stones and silty clay (Fig.6). Its loose structure and strong permeability
 239 facilitate infiltration of surface water. The Wenchuan earthquake aggravated the
 240 deformation of the landslide making deposits more unconsolidated, further reducing
 241 the stability of the landslide mass. During persistent rainfall, surface water infiltrates

242 the landslide slope resulting in increased water pressure within the landslide mass and
243 reduced shear strength on the sliding surface. Thus, rainfall constitutes the primary
244 inducing factor of the upper Taziping landslide. After infiltrating the loose layer, water
245 saturates the slope increasing the dead weight of the sliding mass and reducing the
246 shear strength of soil in the sliding zone. Infiltration into the landslide mass also
247 increases the infiltration pressure of perched water, drives deformation, and poses a
248 great threat to villages located at the front of the landslide. Slide-resistant piles and
249 backfill were placed at the toe of the slope in order to reduce the hazards of future
250 slides. The slide-resistant piles have enhanced the overall stability of the slope,
251 however, under heavy rainfall the upper unconsolidated landslide deposits may cut
252 out from the top of the slide-resistant piles.



253
254 (a) Material on the landslide surface (b) Material in the shear zone

255 Fig.6 Colluvial deposits covers on the mountain slope

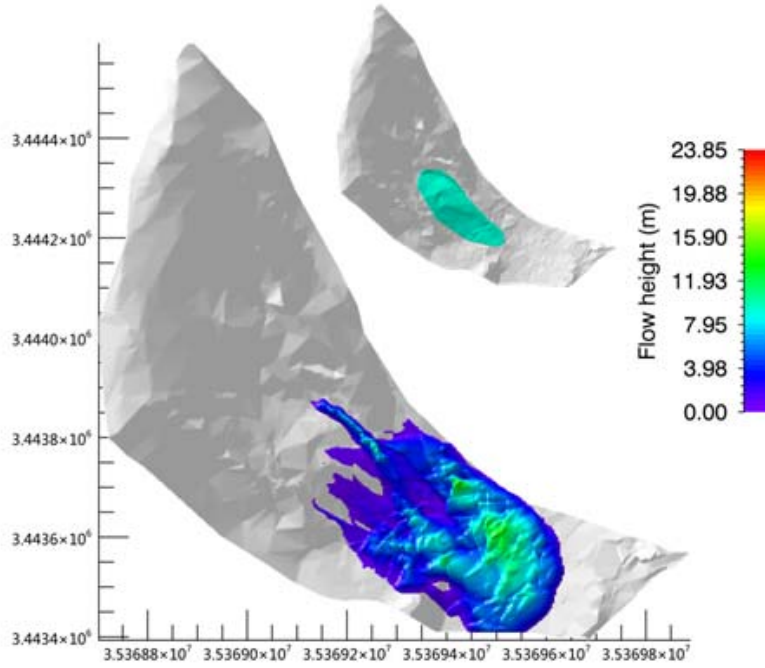
256 Therefore we simulate possible movement states of the Taziping landslide before
257 and after treatment with slide-resistant piles, comparatively analyzed the kinetic
258 parameters in the movement process, and mapped the 2D division of hazard zones.

259 3.2 Hazard prediction before treatment

260 It was assumed that the landslide was damaged before engineering treatment.
261 According to field investigation, the sliding mass had an estimated starting volume of
262 about $600,000\text{m}^3$ and a mean thickness of 8m. Based on the survey report and field
263 investigation (Hydrologic Engineering and Geological Survey Institute of Hebei
264 Province, 2010), we adopted the survey parameters of Tab.2 for the simulated
265 calculation. These parameters obtained from performing laboratory or small-scale
266 experiments and back-analyses of relatively well-documented landslide cases. The
267 unit weigh $\gamma = 20.8\text{kN} \cdot \text{m}^{-3}$ which we used is from small-scale conventional
268 triaxial test experiments in laboratory. In addition, we selected the coulomb friction
269 coefficient $\mu = 0.45$ and viscous friction coefficient $\zeta = 500\text{m} \cdot \text{s}^{-2}$ in accordance
270 with back-analyses of well-documented landslide cases (Cepeda et al., 2010; Du et al.,
271 2015). The erosional entrainment rate selected the minimum value $k_i = 0.0001$ in
272 program RAMMS.
273

Tab.2 Model calculation parameters

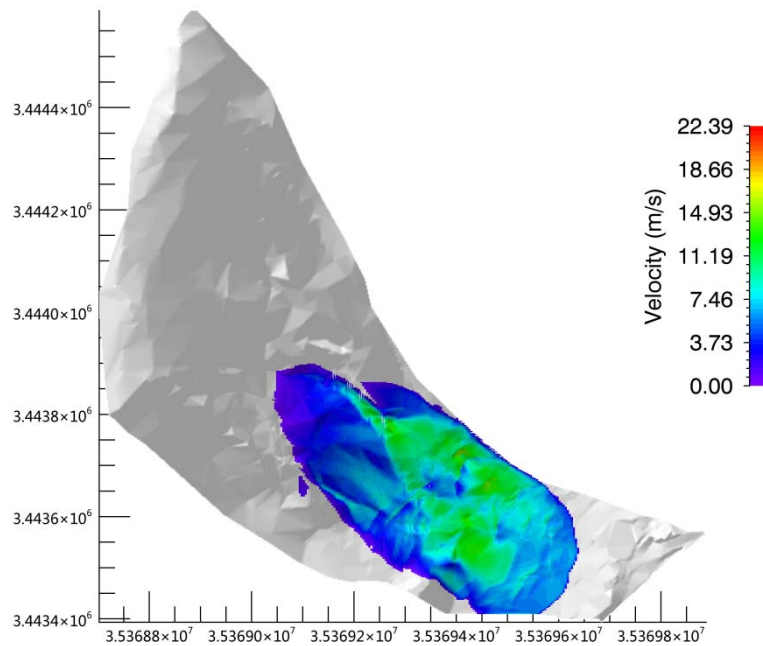
Unit weight $\gamma(kN \cdot m^{-3})$	Coulomb friction coefficient μ	Viscous friction coefficient $\zeta(m \cdot s^{-2})$	Erosional entrainment rate k_i
20.8	0.45	500	0.0001



275

276

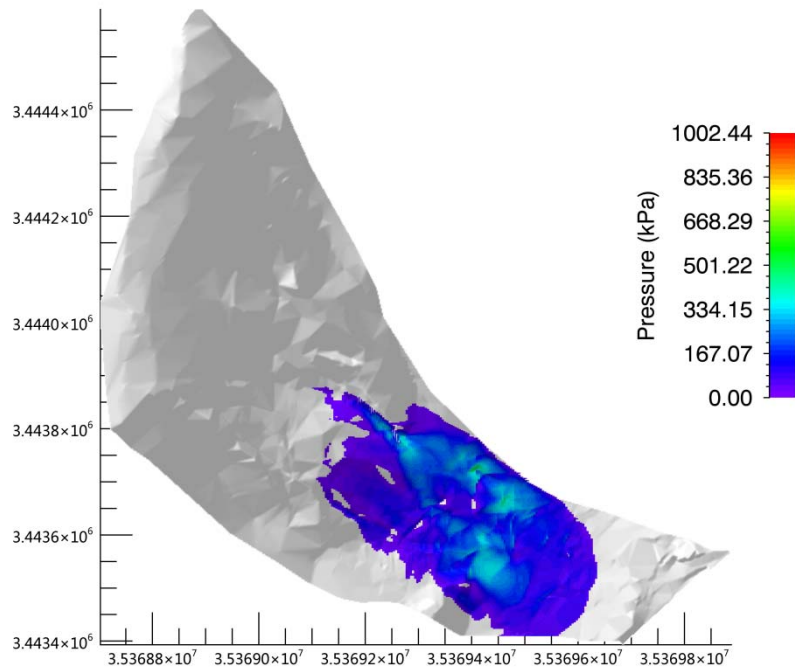
(a) Flow height



277

278

(b) Velocity



(c) Pressure

279

280

281 Fig.7 Movement characteristic parameters of Taziping landslide (before treatment)

282

283

284

285

286

287

288

289

290

291

292

293

294

See the kinematic characteristic parameters of the landslide deposits in Fig.7 The coloredbar shows the maximum values of moving process or an instantaneous for a given time step. As shown by the calculation results, deposits accumulated during the landslide movement process had a maximum flow height of 23.85m, located around the surface gully of the middle and upper slope. The middle and lower of the landslide deposits had a flow height of about 5-10m; the middle and lower movement velocity of the landslide ranged from 3m/s and 7m/s. The landslide had a mean pressure of about 500kPa, and the pressure of the middle and lower deposits was about 200kPa. Thus, three-story and lower houses within the deposition range might be buried, and it was further suggested that the design strength of the gable walls of houses on the middle and upper parts of the deposit be increased above 300kPa.

3.3 Hazard prediction after treatment

295

296

297

298

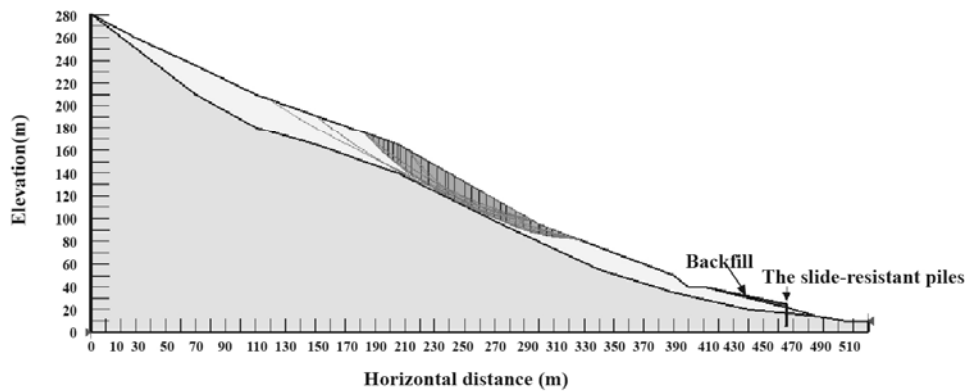
299

300

301

After fully accounting for the slide-resistant piles and mounds, we introduced the Morgenstern-Price method (Morgenstern et al., 1965) to calculate the stability coefficient of Taziping landslide after treatment. The method was determined with an iterative approaching by changing the position of the sliding surface until failure of the dumpsite (Fig.8). The physico-mechanical parameters under a saturated state (Hydrologic Engineering and Geological Survey Institute of Hebei Province, 2010) were adopted to search for the sliding plane of the landslide.

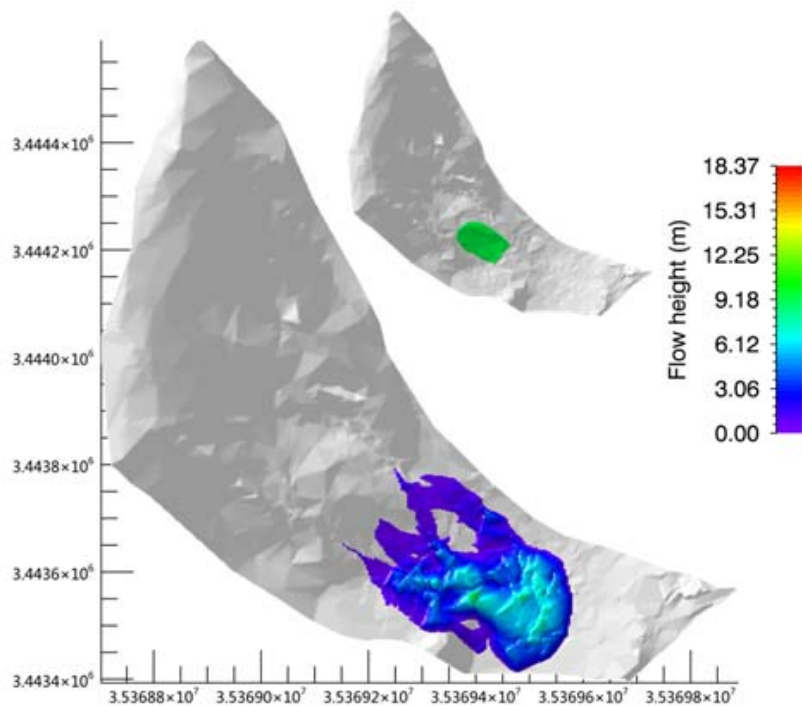
0.998



302

303 Fig.8 Search for the sliding plane of Taziping landslide (before treatment)

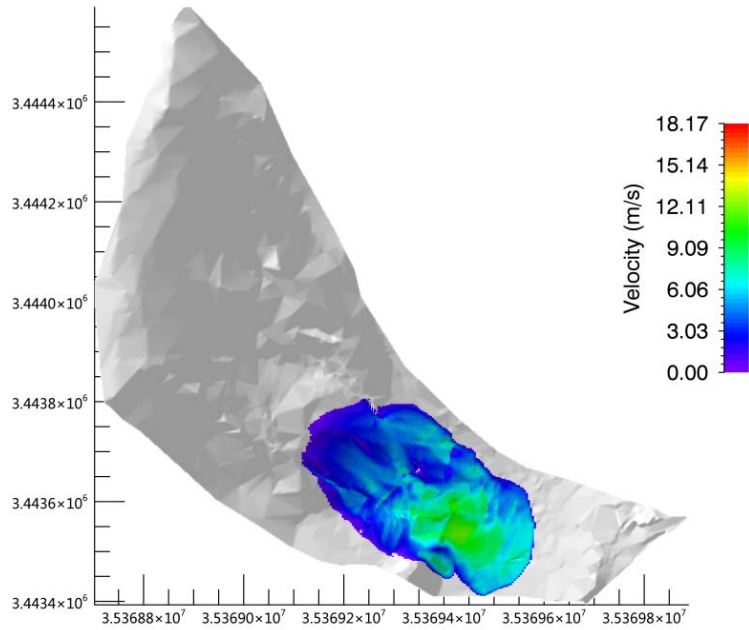
304 Based on the numerical analysis, the Taziping landslide stability coefficient was
305 0.998. it was found under rainfall conditions, the middle area of Taziping landslide was
306 unstable. Loose deposits in the middle part of the landslide might convert into
307 high-water landslide substances and cut out from the top of the slide-resistant piles. In
308 the damaged area, the slope had a rear edge wall elevation of about 1,170m. Its front
309 edge was located on the south side of the mountain road, with an elevation of
310 1,070-1,072m and a length of 182m. Thus, the scale of the rainfall-damaged is
311 estimated to be about 250,000m³, with a mean thickness of about 6m. The parameters
312 in Tab.2 were again adopted for the simulated calculation.



313

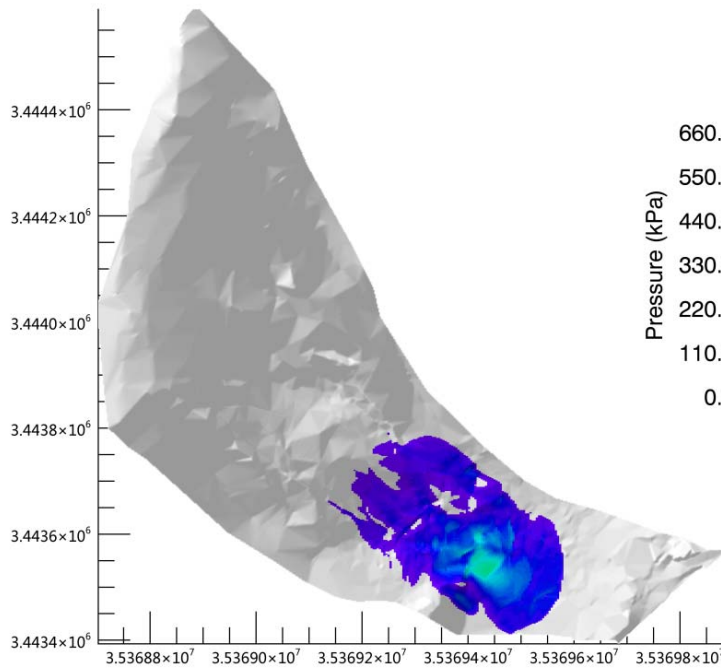
314

(a) Flow height



315
316

(b) Velocity



317
318

(c) Pressure

Fig. 9 Movement characteristic parameters of Taziping landslide (after treatment)

Provided in Fig. 9 are the kinematic characteristics of the landslide deposit. The coloredbar shows the maximum values of moving process or an instantaneous for a given time step. Deposits accumulated during the landslide movement process had a maximum flow height of 18.37m, located around the surface gully of the middle and upper slope. Middle and lower of the landslide deposits had a flow height of approximately 3-5m. The middle and lower movement velocity of the landslide

326 deposits ranged between 3m/s and 5m/s. The landslide had a mean pressure of about
 327 330kPa, and the pressure of the middle and lower deposits was about 100kPa. Thus, it
 328 could be held that two-story and lower houses within the deposition range might be
 329 buried. It was further suggested that the design strength of the gable walls of houses
 330 on the middle and upper parts of the deposits be increased above 150kPa.

331 After treatment, the accumulation flow height and pressure of the deposits were
 332 reduced by about 1/2, and the kinematic speed was reduced by about 1/3. However,
 333 the Miaoba residential area of Red Village was still partially at hazard.
 334

335 4 Results

336 Landslides reflect landscape instability that evolves over meteorological and
 337 geological timescales, and they also pose threats to people, property, and the
 338 environment. The severity of these threats depends largely on landslide speed and
 339 travel distance. There may be examples where entire houses on a landslide mass are
 340 moved but not destroyed because of stable base plates. In any case, velocity plays a
 341 more important role regarding kinetic energy acting on an obstacle. However, the
 342 Miaoba residential area of Red Village is located at the frontal part of Tazhiping
 343 lanslide. Then, during landslide movement, the spatial scale indexes of a landslide
 344 mass include area, volume, and thickness. The maximum thickness of the landslide is
 345 one of the direct factors influencing the building's deformation failure status. A large
 346 landslide displacement may lead to burial, collapse, or deformation failure of the
 347 building, and thus influence its safety and stability. Thus, landslide thickness
 348 constitutes an important index for assessing the hazards of a landslide disaster, and for
 349 influencing the consequences faced by disaster-affected bodies (Fell et al., 2008;
 350 DZ/T, 0286-2015). Provided in Tab.3 is a landslide thickness-based division of the
 351 predicted hazard zones of Taziping landslide, in which the thickness of the landslide
 352 mass correlates with the ability of a building to withstand a landslide disaster (Hungr
 353 et al., 1984; Petrazzuoli et al., 2004; GB, 50010–2010; Hu et al., 2012; Zeng et al.,
 354 2015). After treatment with slide-resistant piles, the hazard of a future slide was
 355 reduced by about 1/3 overall and by 2/3 in high-hazard zones.

356 **Tab.3 Division table of the predicted hazards of Taziping landslide (unit: m²)**

Hazard zone level	Assessment index	Building damage probability	Area before treatment	Area after treatment	Increased/decreased area	Building damage characteristics
Low-hazard zone (I)	$h \leq 0.5\text{m}$	20%	44 , 600	38 , 748	-5,852	One-story houses may be damaged; houses on the

Relatively low-hazard zone (II)	$0.5\text{ m} <$	50~20%	24 , 900	26 , 400	+1,500	landslide mass are partially damaged. One-story houses have a very high probability of being damaged; one-story houses on the landslide mass are completely damaged. One-story to three-story houses have a very high probability of being damaged; houses less than three stories on the landslide mass are completely damaged. One-story houses may be buried, and two-story to six-story houses have a very high probability of being damaged; houses on the landslide mass are completely
	$h \leq 1\text{m}$					
Moderate-hazard zone (III)	$1\text{m} < h \leq 3\text{m}$	80~50%	21 , 980	15 , 856	-6,124	landslide mass are completely damaged. One-story houses may be buried, and two-story to six-story houses have a very high probability of being damaged; houses on the landslide mass are completely
Relatively high-hazard zone (IV)	$3\text{m} < h \leq 5\text{m}$	100~80%	30 , 820	19 , 636	-11,184	landslide mass are completely

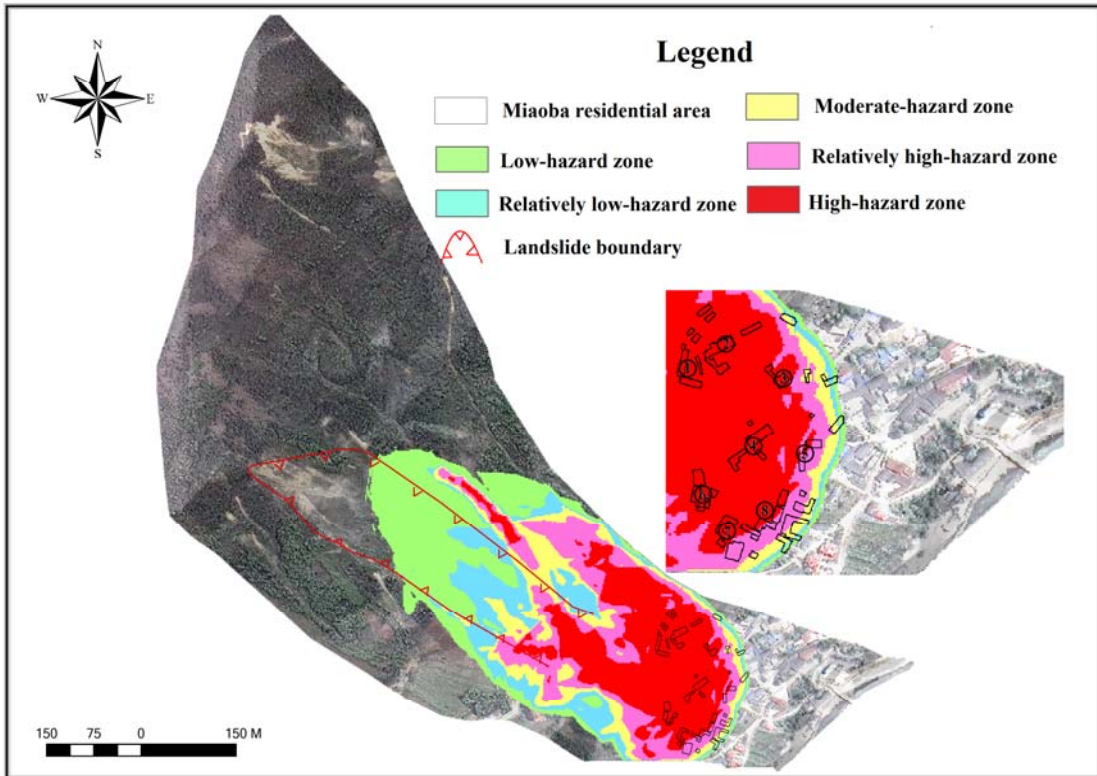
High-hazard

zone	$h \geq 5m$	100%	47 , 240	13 , 052	-34,188
(V)					

Total area:	—	—	169 , 540	113 , 700	-54,340	—
-------------	---	---	-----------	-----------	---------	---

damaged.
 Two-story and lower houses may be buried, and three-story and higher houses have a very high probability of being damaged; houses on the landslide mass are completely damaged.

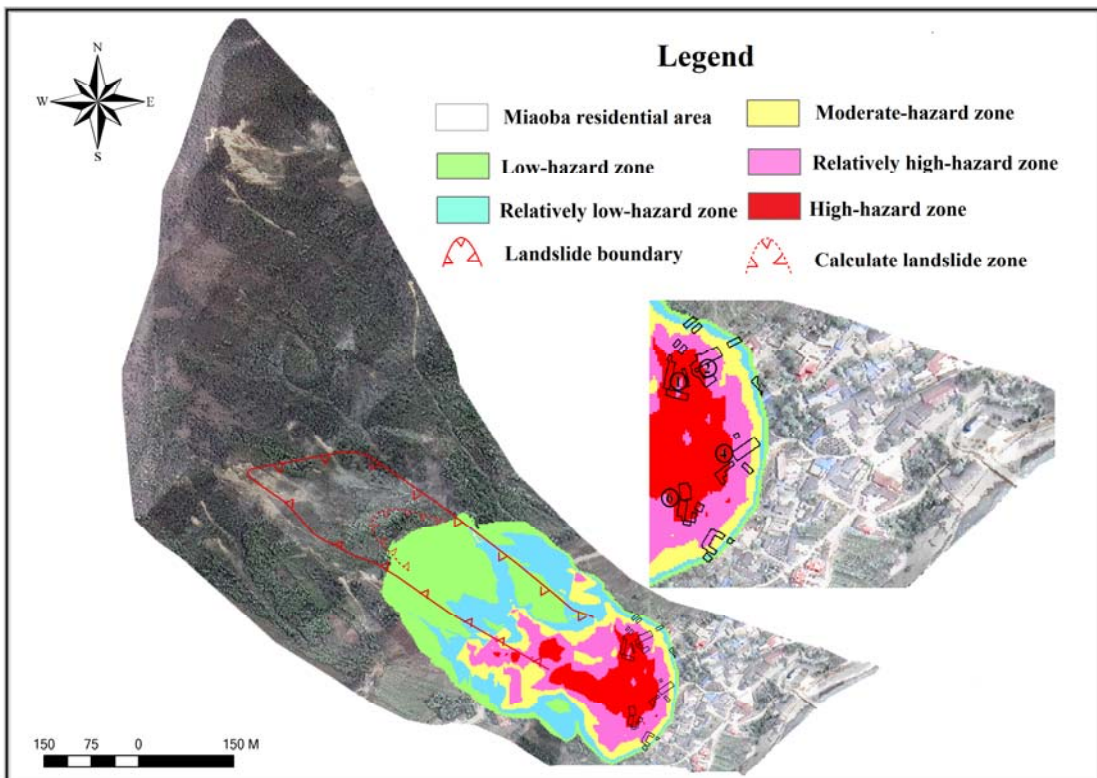
357 Given in Fig.10 are the 2D divisions of hazard zones of Taziping landslide before
 358 and after engineering treatment. The scope of the hazard zones changed before and
 359 after engineering treatment, particularly in the high-hazard zones. Before treatment
 360 with slide-resistant piles, the landslide posed a great hazard to eight houses on the left
 361 side of the upper Miaoba residential area, with high-hazard zone associated with
 362 landslide mass height over 5m and red zone. After treatment, the number of effected
 363 houses was reduced to four. We defined outside the colored area as no-hazard.



364

365

(a) Before treatment



366

367

368

369

(b) After treatment

Fig.10 2D division comparison of the hazards of Taziping landslide

370 5 Conclusions and Discussion

371 The hazard assessment of landslide using numerical models is becoming more
372 and more popular as new models developing and becoming available in both scientific
373 research and practical applications. There is some confusion about the mass
374 movement process that is discussed and approached by the presented and adopted
375 rheological model.

376 On the one hand, Landslides move downslope in many different ways (Varnes,
377 1978). In addition landslides can evolve into rapidly travelling flows, which exhibit
378 characteristics of debris flows on unchannelized or only weakly channelized hillslopes.
379 The geomorphic heterogeneity of rapid shallow landslides such as hillslope debris
380 flows is larger than observed in channelized debris flows, however many of these
381 flows can be successfully modelled using the Voellmy-fluid friction relation and
382 starting the flow as a block release (Christen et al., 2012). This paper simulation
383 results support this option that Voellmy-fluid rheological model can also be used in
384 the simulation of flow-type landslides.

385 On the other hand, The selection of model parameters remains one of the
386 fundamental challenges for numerical calculations in natural hazards. At present, there
387 are a high empirical parameters obtained from 30-year monitoring data on avalanche.
388 Such as in RAMMS, we can automatically generate the friction coefficient of
389 avalanche for our calculation domain based on topographic data analysis, forest
390 information and global parameters and so on (WSL, 2013). The friction parameters of
391 debris flow can found in some literature (Fannin et al., 2001; Iovine et al., 2003;
392 Hürlimann et al., 2008; Scheidl et al., 2010; Huang et al., 2015). However, There are
393 seldom cases researching on friction parameters of flow-type landslide. Therefore, we
394 tested different coulomb friction coefficient μ values ranging between $0.1 \leq \mu \leq 0.6$

395 and viscous friction coefficient ζ values ranging between $100 \leq \mu \leq 1000 m \cdot s^{-2}$.

396 Finally, we selected the coulomb friction coefficient $\mu = 0.45$ and viscous friction

397 coefficient $\zeta = 500 m \cdot s^{-2}$ in accordance with back-analyses of well-documented
398 landslide cases (Cepeda et al., 2010; Du et al., 2015). The results of the simulation
399 results is consistent with the field observation in terms of topography and sliding path.

400 Based on the finite volume method and program RAMMS, the simulation results
401 of Taziping landslide were consistent with the sliding path predicted by the field
402 investigation. This correlation indicates that numerical simulation is an effective
403 method for studying the movement processes of flow-type landslide. The
404 accumulation flow height and pressure of landslide deposits were reduced by about
405 1/2, and the kinematic speed was reduced by about 1/3 after treatment. However, the
406 Miaoba residential area of Red Village is still partially at hazard. Considering that
407 two-story and lower houses within the deposition range might be buried, it was further
408 suggested that the design strength of the gable walls of houses on the middle and
409 upper parts of the deposit be increased above 150kPa.

410 By utilizing a GIS platform in combination with landslide hazard assessment
411 indexes, we mapped the 2D division of the Taziping landslide hazard zones before
412 and after engineering treatment. The results indicated that overall hazard zones
413 contracted after engineering treatment and, the area of high-hazard zones was reduced
414 by about 2/3. After engineering treatment, the number of at hazard houses on the left
415 side of the upper Miaoba residential area, was reduced from eight to four. It was thus
416 clear that some zones are still at high hazard despite engineering treatment. Therefore,
417 it was proposed that houses located in high-hazard zones be relocated or reinforced
418 for protection.

419

420

421

422 **Acknowledgments**

423 First of all, the authors give sincere acknowledgement to CAS Pioneer Hundred
424 432 Talents Program for the completion of this research. This work was supported by
425 National Natural Science Foundation of China (Grant No. 41301009) and the
426 Hundred Young Talents Program of IMHE (SDSQB-2016-01), the International
427 Cooperation Program of the Ministry of Science and Technology of China (Grant
428 No.2013DFA21720). The authors express their deepest gratitude to those aids and
429 assistances. The authors also extend their gratitude to editor and two anonymous
430 reviewers for their helpful suggestions and insightful comments, which have
431 contributed greatly in improving the quality of the manuscript.

432

433

434 **Reference**

435 Bartelt, P., Bühler, Y., Buser, O., Christen, M., and Meier, L.: Modeling massdependent flow
436 regime transitions to predict the stopping and depositional behavior of snow avalanches, *J.*
437 *Geophys. Res.*, 117, F01015, doi:10.1029/2010JF001957, 2012 .

438 Costa, J.E.: Physical geomorphology of debris flows. *Developments and Applications of*
439 *Geomorphology*, Springer Press., 268-317, 1984.

440 Christen, M., Kowalski, J., and Bartelt, P.: RAMMS: Numerical simulation of dense snow
441 avalanches in three-dimensional terrain, *Cold Regions Science and Technology.*, 63, 1–14,
442 2010.

443 Christen, M., Bartelt, P., and Kowalski, J.: Back calculation of the In den Arelen avalanche with
444 RAMMS: interpretation of model results, *Annals of Glaciology.*, 51, 161–168, 2010.

445 Christen, M., Bühler, Y., Bartelt, P., Leine, R., Glover, J., Schweizer, A., Graf, C., McArdell, B.,
446 Gerber, W., Deubelbeiss, Y., Feistl, T., and Volkwein, A.: Integral hazard management using a
447 unified software environment: numerical simulation tool “RAMMS” for gravitational natural
448 hazards, In: Kobltschnig, G., Hübl, J., Braun, J. (eds.) *Proceedings of 12th Congress*
449 *INTERPRAE.*, 1, 77–86, 2012.

450 Chen, J.C., and Chuang, M.R.: Discharge of landslide-induced debris flows: case studies of
451 Typhoon Morakot in southern Taiwan, *Nat. Hazards Earth Syst. Sci.*, 14, 1719-1730, 2014.

452 Cepeda, J., Chávez, J.A., and Martínez, C.C.: Procedure for the selection of runout model

453 parameters from landslide back-analyses: application to the Metropolitan Area of San
454 Salvador, El Salvador, *Landslides*, 7, 105–116, 2010.

455 Du, J., Yin, K.L., and Wang, J.J.: Simulation of three-dimensional movement of landslide-debris
456 flow based on finite volume method, *Chinese Journal of Rock Mechanics and Engineering*,
457 34: 480–488, 2015 (in Chinese).

458 Evans, S.G., Tutubalina, O.V., Drobyshev, V.N., Chernomorets, S.S., McDougall, S., Petrakov,
459 D.A., and Hungr, O.: Catastrophic detachment and high-velocity long-runout flow of Kolka
460 Glacier, Caucasus Mountains, Russia in 2002, *Geomorphology*, 105, 314–321, 2009.

461 Fannin, R.J., and Wise, M.P.: An empirical-statistical model for debris flow travel distance,
462 *Canadian Geotechnical Journal*, 38, 982–994, 2001.

463 Finlay, P.J., Mostyn, G.R., and Fell, R.: Landslide risk assessment: prediction of travel distance,
464 *Canadian Geotechnical Journal*, 36, 556–562, 1999.

465 Fell, R., Corominas, J., Bonnard, C., Cascini, L., Leroi, E., and Savage, W. Z.: Guidelines for
466 landslide susceptibility, hazard and risk zoning for land use planning, *Engineering Geology*,
467 102, 85–98, 2008.

468 Fannin, R., and Wise, M.: An empirical-statistical model for debris flow travel distance, *Can*
469 *Geotech J* ., 38, 982–994, 2001.

470 GB 50010–2010.: Code for design concrete structures, Beijing: Chinese Architectural Industry.,
471 34–80, 2010 (in Chinese).

472 Hebei Province Institute of Hydrogeological and Engineering.: Geological investigation
473 engineering supplemental survey report of Hongse Village Taziping landslide in Hongkou
474 Town of Dujiangyan City, Sichuan Province., 2010 (in Chinese).

475 Hungr, O.: A Model for the runout analysis of rapid flow slides, debris flows and avalanches, *Can*
476 *Geotech J* ., 32, 610–623, 1995.

477 Hungr, O., Evans, S.G., Bovis, M.J., and Hutchinson, J.N.: A review of the classification of
478 landslides of the flow type, *Environ Eng Geosci*, 7, 221–238, 2001.

479 Hungr, O., Morgan G.C., and Kellerhals, R.: Quantitative analysis of debris torrent hazards for
480 design of remedial measures, *Can Geotech J.*, 21, 663–677, 1984.

481 Hu, K.H., Cui, P., and Zhang, J.Q., Characteristics of damage to buildings by debris flows on 7
482 August 2010 in Zhouqu, Western China, *Nat Hazards Earth Syst Sci.*, 12, 2209–2217, 2012.

483 Hürlimann, M., Rickenmann, D., Medina, V., and Bateman, A.: Evaluation of approaches to
484 calculate debris-flow parameters for hazard assessment, *Eng Geol.*, 102, 152–163, 2008.

485 Huang, Y., Cheng, H., Dai, Z., Xu, Q., Liu, F., Sawada, K., Moriguchi, S., and Yashima, A.:
486 SPH-based numerical simulation of catastrophic debris flows after the 2008 Wenchuan
487 earthquake, *Bull Eng Geol Environ.*, 74, 1137–1151, 2015.

488 Iverson, R. M., Reid, M. E., and LaHusen, R. G.: Debris-flow mobilization from landslides, *Annu.*
489 *Rev. Earth Planet Sc.*, 25, 85– 138, 1997.

490 Iverson, R.M., and Vallance, J.W.: New views of granular mass flows, *Geology*, 29, 1115–1118,
491 2001.

492 Iovine, G., Gregorio, S.D., and Lupiano, V.: Debris-flow susceptibility assessment through cellular
493 automata modeling: an example from 15–16 December 1999 disaster at Cervinara and San
494 Martino Valle Caudina (Campania, southern Italy), *Nat Hazards Earth Syst Sci.*, 3, 457–468,
495 2003.

496 Jackson, L.E., Kostashuk, R.A., and MacDonald, G.M.: Identification of debris flow hazard on

497 alluvial fans in the Canadian Rocky mountains, Geological Society of America., 7, 155–124,
498 1987.

499 LeVeque, R.: Finite Volume Methods for Hyperbolic Problems, Cambridge Texts in Applied
500 Mathematics Cambridge University Press., 2002.

501 Michael-Leiba, M., Baynes, F., Scott, G., and Granger, K.: Regional landslide risk to the Cairns
502 community, NatHazards., 30, 233–249, 2003.

503 Morgenstern, N.R., and Price, V.E.: The analysis of the stability of general slip surfaces,
504 Geotechnique., 15, 79–93, 1965.

505 Portilla, M., Chevalier, G., and Hürlimann, M.: Description and analysis of the debris flows
506 occurred during 2008 in the Eastern Pyrenees, Nat. Hazards Earth Syst. Sci., 10, 1635–1645,
507 2010.

508 Petrazzuoli, S.M., and Zuccaro, G.: Structural resistance of reinforced concrete buildings under
509 pyroclastic flows: a study of the Vesuvian area, J Volcanol Geoth Res., 133, 353–367, 2004.

510 Sassa, K., Nagai, S., Solidum, R., Yamazaki, Y., and Ohta, H.: An integrated model simulating the
511 initiation and motion of earthquake and rain induced rapid landslides and its application to
512 the 2006 Leyte landslide, Landslides., 7, 219–236, 2010.

513 Scott, K.M., and Vallance, J.W.: History of Landslides and Debris Flows at Mount Rainier: Water
514 Fact Sheet, USGS Open-File Report., 93–111, 1993.

515 Shi, G.H.: Discontinuous deformation analysis - a new numerical model for the statics and
516 dynamics of block system, Berkeley: University of California., 1988.

517 DZ/T 0286-2015.: Specification of risk assessment for geological hazard, Ministry of Land and
518 Resources of the People's Republic of China., 2015 (in Chinese).

519 Scheidl, C., and Rickenmann, D.: Empirical prediction of debris-flow mobility and deposition on
520 fans, Earth Surf Proc Land., 35, 157–173, 2010.

521 Toro, E.F.: Riemann problems and the waf method for solving the two dimensional shallow water
522 equations. Philos. Trans. R. Soc. London., Ser. A 338, 43–68, 1992.

523 Varnes, D.J., : Slope movement types and processes. In: Schuster RL, Krizek RJ (eds) Landslides:
524 analysis and control. Transportation Research Board, National Research Council, Washington,
525 DC, USA., 11–33 , 1978.

526 Wang, L., Li, B., Gao, Y., and Zhu, S.: Run-out prediction of large thick-bedded unstable rock: A
527 case study of Daxiang unstable rock in Yangjiao town, Wulong county, Chongqing, Earth
528 Science Frontiers., 23, 251–259, 2016 (in Chinese).

529 WSL.: RAMMS: A numerical model for snow avalanches in research and practice, User manual
530 v1.5 avalanche, WSL Institute for snow and avalanche research SLF, Swiss., 2013.

531 Zeng, C., Cui, P., Su, Z.M., Lei, Y., Chen, R.: Failure modes of reinforced concrete columns of
532 buildings under debris flow impact, Landslides., 12, 561-571, 2015.